

pubs.acs.org/acschemicalbiology Article

Design, Synthesis, and Mechanistic Studies of (R)-3-Amino-5,5-difluorocyclohex-1-ene-1-carboxylic Acid as an Inactivator of Human Ornithine Aminotransferase

Allison N. Devitt,[#] Abigail L. Vargas,[#] Wei Zhu, Benjamin James Des Soye, Fatma Ayaloglu Butun, Tyler Alt, Nicholas Kaley, Glaucio M. Ferreira, Graham R. Moran, Neil L. Kelleher, Dali Liu, and Richard B. Silverman*



Cite This: ACS Chem. Biol. 2024, 19, 1066-1081



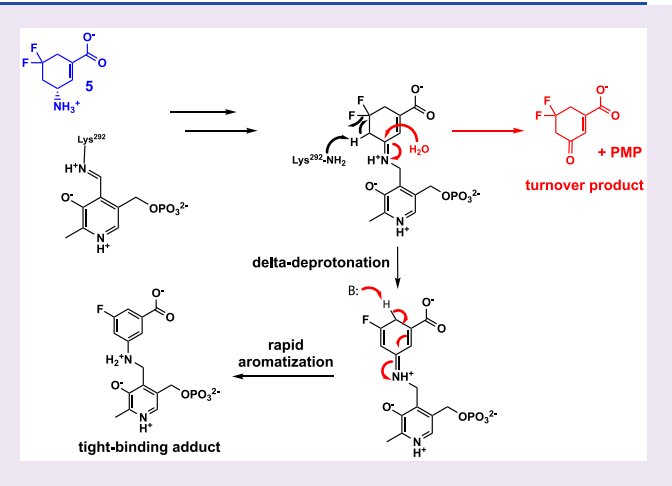
ACCESS

III Metrics & More

Article Recommendations

Supporting Information

ABSTRACT: Human ornithine aminotransferase (hOAT), a pyridoxal 5'-phosphate (PLP)-dependent enzyme, has been shown to play an essential role in the metabolic reprogramming and progression of hepatocellular carcinoma (HCC). HCC accounts for approximately 75% of primary liver cancers and is within the top three causes of cancer death worldwide. As a result of treatment limitations, the overall 5-year survival rate for all patients with HCC is under 20%. The prevalence of HCC necessitates continued development of novel and effective treatment methods. In recent years, the therapeutic potential of selective inactivation of hOAT has been demonstrated for the treatment of HCC. Inspired by previous increased selectivity for hOAT by the expansion of the cyclopentene ring scaffold to a cyclohexene, we designed, synthesized, and evaluated a series of novel fluorinated cyclohexene analogues and identified (R)-3-amino-5,5-difluorocyclohex-1-ene-1-carboxylic acid as a time-dependent inhibitor of hOAT. Structural and mechanistic



studies have elucidated the mechanism of inactivation of hOAT by 5, resulting in a PLP-inactivator adduct tightly bound to the active site of the enzyme. Intact protein mass spectrometry, ¹⁹F NMR spectroscopy, transient state kinetic studies, and X-ray crystallography were used to determine the structure of the final adduct and elucidate the mechanisms of inactivation. Interestingly, despite the highly electrophilic intermediate species conferred by fluorine and structural evidence of solvent accessibility in the hOAT active site, Lys292 and water did not participate in nucleophilic addition during the inactivation mechanism of hOAT by 5. Instead, rapid aromatization to yield the final adduct was favored.

INTRODUCTION

Hepatocellular carcinoma (HCC) accounts for around 75% of primary liver cancers and is among the three most common causes of cancer death worldwide.^{1–4} Currently, the most effective treatment for early-stage HCC is a liver transplant, with a 5-year survival rate greater than 75%.⁵ However, liver grafts are in limited supply, resulting in strict criteria for who can receive a transplant, and wait times greater than 2 years in some parts of the US are typical.^{6,7} Common bridge and late-stage treatments include surgical removal of tumors, chemotherapy, and immunotherapy, all of which have potential harmful side effects. Unfortunately, the recurrence rate of HCC is about 80% following tumor resection;⁵ thus, this treatment option is largely only effective as a palliative measure. As a result of limited treatment options, the overall 5-year survival rate for all patients with HCC is under 20%.⁸

The prevalence and lethality of HCC necessitates the development of new effective treatment options.

In recent years, human ornithine aminotransferase (*h*OAT) has been demonstrated to play an important role in the metabolic reprogramming and progression of HCC. *h*OAT is a pyridoxal 5'-phosphate (PLP)-dependent enzyme involved in the biosynthesis of amino acids glutamine and proline. Structurally, *h*OAT has a type-I aminotransferase fold and homodimeric biological assembly with two active sites located at the dimer interface. Prior to catalysis, the PLP cofactor is

Received: January 10, 2024 Revised: February 18, 2024 Accepted: March 8, 2024 Published: April 17, 2024





Scheme 1. Half-Reactions of hOAT and Metabolic Reprogramming in HCC

stabilized in the active site through formation of a Schiff base with a conserved catalytic lysine residue (Lys292 in hOAT) along with other noncovalent interactions, including those with the neighboring subunit. hOAT has a Ping Pong bi-bi mechanism to facilitate the transfer of the δ -amino group from L-ornithine to α -ketoglutarate (α -KG) to produce glutamate-5-semialdehyde (GSA) and L-glutamate (L-Glu), respectively (Scheme 1).11 In the first half-reaction, ornithine serves as the amino donor and is converted to GSA. PLP serves as the amino acceptor and is thus converted to pyridoxamine-5'-phosphate (PMP). The resulting GSA then spontaneously cyclizes to 1-pyrroline-5-carboxylate (P5C), which can be converted to proline by pyrroline-5-carboxylate reductase (PYCR). In the second half-reaction, PLP is regenerated from PMP following the transfer of the amino group to α -KG to yield L-Glu, which can also be converted to P5C by pyrroline-5-carboxylate synthase (P5CS).¹⁰ Recently, there has been a growing interest in proline metabolism as a therapeutic target for a variety of cancers, as proline metabolism appears to play an important role in metabolic reprogramming that sustains cancer proliferation (Scheme 1).9,13 Specifically, changes in the expression of P5CS and PYCR are associated with promoting cancer cell growth and resistance to apoptosis.¹⁴ The metabolic reprogramming in HCC, similar to other cancers, is characterized by activation of the proline/ hydroxyproline pathway. 15 This supports hypoxia-inducible factor- 1α (HIF1 α)-dependent tumor progression and plays a key role in HCC's resistance to sorafenib, explicitly regarding vasculogenic mimicry. 15 Upregulation of biosynthetic pathways of other amino acids, such as glutamine, can also support unregulated cell growth, 9,16,17 as malignant tumor cells utilize a greater abundance of glutamine to sustain proliferation. The glutamate produced by hOAT can be converted to glutamine (L-Gln) via glutamine synthetase (GS). hOAT and other glutaminogenic enzymes are highly activated and often overexpressed in HCC due to aberrant, oncogenic Wnt/ β -catenin signaling. Thus, selective inactivation of hOATdemonstrates therapeutic potential in the treatment of HCC and related cancers. Among the 14 known aminotransferase enzymes in humans, hOAT belongs to the same evolutionary subgroup 20,21 as $\gamma\text{-aminobutyric}$ acid aminotransferase (GABA-AT). This subgroup is defined by the transfer of an amino group that is distant from the α -carbon, instead of the α -amino group (Scheme 2). 22,23 In the cases of hOAT and GABA-AT, these enzymes catalyze the transfer of the δ and γ -amino groups of L-ornithine and γ -aminobutyric acid (GABA), respectively. The active sites of hOAT and GABA-AT share a high degree of similarity, with only active site residues Tyr85

Scheme 2. hOAT and GABA-AT Half-Reactions

and Tyr55 in hOAT being replaced by Ile72 and Phe351, respectively, in GABA-AT. Tyr55 in hOAT is proposed to be a key binding residue for substrate ornithine; the α -amino group of ornithine is hydrogen-bonded to Tyr55, leaving the δ amino group to form a Schiff base with PLP. 23

Our laboratories have been developing rationally designed mechanism-based inactivators (MBIs) to inactivate GABA-AT as a potential treatment for epilepsy and drug addiction.²⁴ An MBI is designed to act initially as a substrate for a target enzyme, which catalytically generates an intermediate that leads to inactivation of that enzyme.²⁵ This inactivation process is functionally irreversible, forming either a covalently bound or tightly bound noncovalent adduct to the enzyme. Ideally, MBIs are inert until they engage with an active site of a specific target enzyme, avoiding the risk of undesirable offtarget interactions and unintended effects. Due to the high similarity of the active sites and enzymatic mechanisms of hOAT and GABA-AT, some of the MBIs initially designed to inactivate GABA-AT have also been shown to inactivate hOAT. Examples of this include CPP-115 and OV329, although both GABA-related compounds more readily inactivate GABA-AT than hOAT.²⁶⁻²⁸ Other MBIs were found to be selective for hOAT over GABA-AT, such as

Figure 1. Structures of selective hOAT inactivators and substituted analogues.

Scheme 3. Proposed Mechanisms of Inactivation of hOAT by 5

(1S,3S)-3-amino-4-(hexafluoropropan-2-ylidenyl)-cyclopentane-1-carboxylic acid,²⁹ which is highly selective for hOAT over GABA-AT.²⁸

Our more recent efforts focus on improving the potency and selectivity of MBIs toward hOAT over other aminotransferase enzymes. We have found that by expanding the cyclopentene scaffold previously developed for GABA-AT inactivators to a series of cyclohexene analogues, such as (S)-3-amino-4,4-difluorocyclohex-1-ene-1-carboxylic acid (1), designed to take advantage of the larger and more accommodating active site of hOAT over that of GABA-AT, improved potency and selectivity for hOAT have been realized. $^{30-33}$ We also reported recently that a second δ -deprotonation step required in the inactivation mechanism of (3S,4R)-3-amino-4-(difluoromethyl)cyclopent-1-ene-1-carboxylic acid (2) provided high selectivity for hOAT over GABA-AT, while analogues that did not utilize a second deprotonation step were unselective. 34

Herein, we describe hOAT inactivation with a set of potential mechanism-based inactivators (Figure 1). The inhibitory potency of these inactivators is characterized, and the mechanism of inactivation for the inactivator most selective toward hOAT (R)-3-amino-5,5-difluorocyclohex-1-ene-1-carboxylic acid (5) is reported. We considered three potential inactivation pathways for 5 (Scheme 3) and present mass

spectral, X-ray crystallographic, and NMR spectral data to identify the most plausible mechanistic pathway.

■ RESULTS AND DISCUSSION

Design of Novel hOAT Inactivators. The mechanism of inactivation of aminotransferase enzymes by MBIs frequently begins with the MBI engaging the enzyme in a manner like that of the native substrate, i.e., formation of a PLP-inactivator complex (6) to give an external aldimine intermediate (7, Scheme 3). Following deprotonation, the ligand-PLP complex then proceeds through a quinonoid intermediate (8), which rearomatizes to produce a ketimine intermediate (9). We previously showed that the ketimine is more stable in the active site of hOAT than GABA-AT,³² allowing the inactivator to readily react with hOAT, thereby favoring an inactivation pathway over noninhibitory hydrolysis pathways. Compound 5 was designed to undergo a second deprotonation event at the δ -position after forming the initial ketimine intermediate complex (9). We posited that the δ -position would be influenced by the adjacent fluorines and imine, thereby enhancing the acidity of the δ -proton and promoting its abstraction. A subsequent elimination of one of the fluoride ions would then provide an intermediate species (10) that could have at least three fates: pathway a, aromatization to 11, or nucleophilic substitution by Lys292 (pathway b) or water (pathway c) with loss of the second fluoride ion. Aromatization

Scheme 4. Synthesis of Analogues 4 and 5^a

"Conditions and Reagents: (a) I₂, overnight (b) DBU; (c) N-bromoacetamide; (d) Bu₃SnH, AIBN, 80 °C, overnight; (e) HCl, MeOH, 40 °C, overnight; (f) PCC, DCM, overnight; (g) DAST, DCM, 50 °C, 3 h; (h) 3 M HCl, MeOH, 75 °C, 2 d; (i) TFAA, DCM, overnight (j) KHMDS, PhSeBr, THF then MCPBA, DCM (k) HCl (aq., 6 M), 90 °C, overnight.

of intermediates 12 and 14 produces 13 and 15, respectively. Pathway b results in covalent inactivation of hOAT, whereas pathways a and c lead to the formation of tightly bound inactivator-cofactor adducts that inactivate hOAT and are unlikely to be released from the pocket on a biologically relevant time scale.

To evaluate the potential for the initial deprotonation of the external aldimine intermediate for both 5 and 4, molecular docking studies were employed (Figures S1 and S2). In hOAT, the external aldimine intermediates of both 5 and 4 showed similar binding poses, with the carboxylate of the inactivator moiety forming stable hydrogen bonds with Arg180. However,

only 5 formed an additional hydrogen bond with Tyr55. Both structures showed the γ -proton was in close proximity to Lys292 (3.0 Å for 5 and 3.2 Å for 4) suggesting that the formation of the ketimine is reasonable. Next, the δ -deprotonation was evaluated. The modeling of the ketimine intermediate for both 5 and 4 predicted that Lys292 would be near the δ -hydrogen of the intermediate, suggesting both should be capable of undergoing the second elimination (3.5 Å for 5 and 3.0 Å for 4).

Syntheses of Substituted Analogues. The synthesis of 5 begins with a previously reported iodolactonization of *R*-(+)-3-cyclohexenecarboxylic acid (16), followed by elimina-

Scheme 5. Synthesis of Analogues^a

OH

$$A, b, c$$
 A, b, c
 A, c

"Conditions and reagents: (a) Rh/Al₂O₃, H₂ (400 psi), 90 °C, overnight; (b) SOCl₂, MeOH, r.t.; (c) Boc₂O, NaHCO₃, MeOH, r.t.; (d) PCC, DCM, overnight, r.t.; (e) DAST, 1,2-dichloroethane, 40 °C, overnight; (f) 4 M HCl, AcOH, 80 °C, overnight.

Table 1. Kinetic Constants for the Inactivation of hOAT and hGABA-AT

	hOAT			hGABA-AT		
compound	K _I (mM)	$k_{\rm inact}~({\rm min}^{-1})$	$k_{\rm inact}/K_{\rm I}~({\rm mM}^{-1}~{\rm min}^{-1})$	K _I (mM)	$k_{\rm inact}~({\rm min}^{-1})$	$k_{\rm inact}/K_{\rm I}~({\rm mM}^{-1}~{\rm min}^{-1})$
5	0.27 ± 0.07	0.28 ± 0.1	1.04	a	a	0.17
4	1.2 ± 0.4	0.15 ± 0.02	0.11	a	<u></u> _a	0.12
(±) 3	no inhibition up to 10 mM			weak reversible inhibition at 10 mM		

 ${}^{a}K_{l}$ and k_{inact} unable to be determined for weak inactivation.

tion of the iodine with DBU to form 17 (Scheme 4).35,36 Compound 17 was then allowed to react with Nbromoacetamide, yielding lactone 18,37 which was then debrominated with tributyltin hydride in the presence of catalytic AIBN at reflux to access lactone 19. Lactone 19 was opened with HCl in methanol at 40 °C overnight to yield alcohol 20 in quantitative yields. Alcohol 20 was able to be used without further purification; however, it has good solubility only in alcohols and water. Oxidation of 20 with PCC in DCM provided ketone 21 as a light green solid in 68% yield with trace chromium contamination. To achieve good yields, multiple extractions with ethyl acetate from an acidic aqueous phase were required. The yield is also highly dependent on 20 being well dispersed and suspended in the reaction solution due to the insolubility of 20 in DCM. Difluorination of 21 with DAST provided 22 in moderate yields along with vinyl fluoride 23. These fluorinated products were challenging to separate with the acetyl-protecting group; consequently, they were moved forward as a mixture. Deprotection of the acetyl group was performed on a mixture of 22 and 23 with 4 M HCl in methanol at reflux over 2 days. The resulting solution was directly concentrated and resuspended in DCM and stirred with an excess of trifluoroacetic anhydride overnight. The two resulting trifluoroprotected analogues of 22 and 23 were readily separable, and 24 was cleanly isolated in 25% yield over the three steps. Improved yields would likely be obtained by improving the acetyl deprotection, which was slow and did not go to completion. However, the method described provided sufficient material to advance the synthesis. Selenation α to the ester was performed, and the subsequent elimination with mCPBA furnished a mixture of unsaturated esters 25 and 26 in 56% yield over two steps. The resulting regioisomers, which showed modest separation via reversed-phase chromatography, were characterized by 2D NMR spectroscopy and X-ray crystallography to confirm their absolute stereochemistry. Previous work on similar scaffolds had shown that with a

Boc protecting group the amine can cyclize onto the ester to form a lactam under these conditions. Due to the electron-withdrawing effects of the trifluoroacetamide group, this was not observed in this system. When the Boc-protected analogue of 24 was used, formation of the lactam was observed along with a variety of other products, and the Boc-protected analogues of 25 and 26 were not readily separated. Global deprotection of both 25 and 26 was achieved by refluxing in aqueous 4 M HCl to yield the desired HCl salts 4 and 5, which were purified via C18 reversed-phase chromatography and accessed in 34 and 87% yields, respectively.

The racemic synthesis of the unsaturated analogues began with the diastereoselective hydrogenation of 3-amino-5-hydroxybenzoic acid hydrochloride 27 with rhodium on alumina to provide 28 as a single diastereomer. The acid was converted to the methyl ester by generating HCl with thionyl chloride in methanol. Lastly, the material was Boc-protected to afford racemic alcohol 28 in 37% yield over three steps. Oxidation of the alcohol group on 28 with PCC provided ketone 29 in 80% yield, which was then subjected to DAST to provide difluorinated intermediate 30 in 59% yield. Global deprotection of 30 provided saturated analogue (±) 3 (Scheme 5).

Kinetic Studies of Analogues. Of the analogues studied, in vitro experiments demonstrated 5 had the greatest inhibitory effect against hOAT (Table 1) with an overall efficiency ($k_{\text{inact}}/K_{\text{I}}$) of 1.04 mM $^{-1}$ min $^{-1}$ (Figure S3). In addition, 4 displayed much weaker inactivation effects against both hOAT and hGABA-AT with $k_{\text{inact}}/K_{\text{I}}$ values 10-fold less effective than that of 5 for hOAT (Figure S4). The double bond appears critical for inactivation, as the saturated analogue ((\pm) 3) displayed little or no inhibitory effect against hOAT or hGABA-AT.

Effects of the Endocyclic Alkene on the pK_a of the δ-Proton. Based on prior work, ²⁶ we expected that the presence of the α , β -unsaturated alkene in 5 compared to 4 and (±) 3 may have a significant influence on the acidity on both the γ -and δ -positions. The proposed mechanisms of inactivation

$$F = 6.33$$

$$-O =$$

Figure 2. Theoretical p K_a 's of γ and δ protons.

include two deprotonation events: first at the γ -position of the inactivator on the aldimine, and then the δ -position of the ketimine. It is common for the γ -deprotonation event, which initiates the inactivation mechanism, to be rate-limiting. However, in this mechanism, another plausible rate-limiting step is the δ -deprotonation event. Regardless of which step is rate-limiting, the pK_a of these two protons will play a critical role in the potency of these potential inactivators and their ability to engage with the target enzyme. To evaluate the effect of the unsaturation on the acidity of these protons, we applied theoretical pK_a calculations for the corresponding intermediate states using the hybrid DFT/B3LYP method in Gaussian09 (Figure 2). The proposed aldimine of the saturated analogue (32) had a much higher theoretical p K_a (8.6) for the γ -proton compared to the unsaturated analogues (6 and 31), indicative of the necessity for installation of the double bond to promote inactivation. When comparing 5 and 4, a significant difference in the theoretical p K_a was observed for both the γ -proton of the aldimine (6.33 vs 7.73) and δ -proton of the ketimine (6.91 vs 7.62). Based on the modeling studies shown in Figures S1 and S2, the binding poses and distances between the catalytic Lys292 and the γ/δ protons for the deprotonation steps of both 4 and 5 are similar. This suggests that the observed difference in activity between 4 and 5 is affected, in large part, by the relative acidity of these protons.

X-ray Crystallography of hOAT Inactivated by 5. To examine the inactivated enzyme-5 complex directly, an X-ray crystal structure of hOAT inactivated by 5 was obtained. Following complete, irreversible inactivation of hOAT by 5, hOAT crystals were grown over 7 days which diffracted to 1.61 Å resolution. The structure of the hOAT-5 inactivated complex was solved utilizing a monomer from a previously published structure of hOAT (PDB code: 6 V8C) as the starting model for molecular replacement. Following model building and refinement cycles, the refined molecular model contained three monomers in one asymmetric unit in the $P3_221$ space group with $R_{\rm free}/R_{\rm work}$ values of 19.30/16.42% (Table S1). The homodimeric biological assembly of hOAT was reconstructed by the addition of a crystallographically symmetric monomer

to give an observed monomer in the asymmetric unit (Figure S5).

The observed electron density clearly supports an inactivator covalently linked to PLP (Figure 3). The observed electron density demonstrates that the binary complex is detached from Lys292 and other active site residues, excluding *pathway b* as a possible mechanism for inactivation. The oxygen atoms on the carboxylate group of the inactivator are stabilized through a hydrogen bonding network with Tyr55 and Arg180, whose native functions are to interact with the α -amino group and the

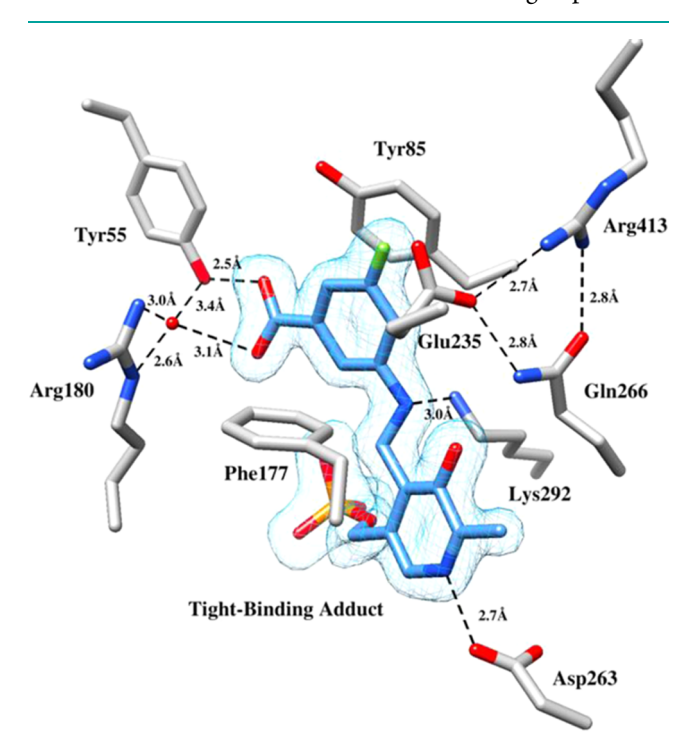


Figure 3. Polder map $(F_o.F_c)$ at 4.0 σ of the final adduct of hOAT inactivated by **5** (PDB ID: 8 V9M). The green atom in the adduct is either a fluorine atom or a hydroxyl group.

 α -carboxylate group of ornithine, respectively.²² One carboxyl oxygen atom forms a strong hydrogen bond (2.5 Å) with Tyr55, and the other oxygen atom maintains an indirect hydrogen bonding interaction with both Tyr55 and Arg180 through an ordered water. Interestingly, a previously published crystal structure of 5-aminovaleric acid complexed with hOAT displayed a nearly identical stabilization of the carboxylate with Tyr55, Arg180, and a water molecule (Figure S6).³⁸ 5-Aminovaleric acid is a slow-binding alternate substrate for hOAT and has been reported to bind in a different orientation compared with ornithine due to lack of an α -amino group. Tyr55 plays a distinct role in the accommodation of the charged α -amino group of ornithine in the active site of hOAT when compared to the hydrophobic residue Phe351 in GABA-AT. 22 Therefore, the strong interaction of carboxylate in this cyclic GABA analogue with Tyr55 is highly important for the selectivity of 5 for hOAT over GABA-AT.

In two of the monomers within the same asymmetric unit, the Glu235-Arg413 salt bridge is partially disrupted but remains intact in one of the monomer copies. This salt bridge is proposed to function as a molecular switch between the first and second half-reactions, preventing nonproductive interaction between Arg413 and the carboxylate group of ornithine in the first half-reaction. ²² In the copies displaying the partially disrupted salt bridge, the side chain of Arg413 has rotated away from Glu235, most likely a result of the bulky cyclohexene ring scaffold of the inactivator.

Mass Spectrometry and ¹⁹F NMR Analysis of the Adduct Formed When hOAT is Inactivated by 5. The crystal structure of 5 bound to hOAT (Figure 3) does not differentiate pathway a from pathway c because of the inability to differentiate a fluorine atom from a hydroxyl group at that resolution. Mass spectrometry, however, might differentiate those possibilities. To confirm irreversible inactivation of hOAT by 5, a time-dependent reactivation experiment (dialysis) was performed. After hOAT activity was partially or fully decreased with 0.6-10 equiv of 5, the samples were dialyzed. Aliquots at different time intervals were collected and assayed to detect restored enzyme activity. No enzymatic activity was recovered after 72 h of dialysis (Figure S7), indicating complete irreversible inhibition of hOAT by 5 on an enzymatically relevant time scale. It takes approximately 10 equiv of 5, however, to produce complete enzyme inactivation.

Intact protein MS was utilized to distinguish between a potential covalent (pathway b) or tight-binding (pathway a or c) inactivation mechanisms for hOAT by 5. Using native topdown protein mass spectrometry, the molecular mass of native hOAT was compared to the molecular mass of hOAT after complete inhibition by 5. A mass shift was observed that corresponded to the addition of the inhibitor, confirming that the inhibitor was bound to the protein/PLP complex (Figure S8). Next, a sample of hOAT inactivated by 5 was denatured, releasing the cofactor and any other small molecules not covalently bound to the enzyme. Upon denaturation, the molecular mass of the native enzyme and inactivated enzyme were equivalent (Figure S9), demonstrating that the inactivator was not covalently bound to hOAT but instead had formed a tight-binding adduct, as also was indicated by the X-ray crystal structure. Thus, pathway b, in which Lys292 is covalently bound to the inactivator moiety to form a ternary adduct, was eliminated as a plausible mechanism of inactivation. However, due to the limited resolution of the intact protein MS, the exact

molecular mass of the adduct could not be determined, and pathways a and c could not be differentiated by these methods.

To determine if fluorine was contained in the inactivated enzyme adduct, ¹⁹F NMR spectroscopy was employed. The ¹⁹F NMR spectra of native hOAT, hOAT inactivated by 5 and dialyzed, and 5 inactivated hOAT denatured with formic acid were compared (Figure S10). Trifluoroethanol was utilized as an internal standard. The NMR spectrum of the native enzyme showed no ¹⁹F peaks, demonstrating the expected absence of fluorine. The spectrum of the inactivated enzyme showed a single peak at -121.7 ppm, indicative of a single fluorine atom bound to the final adduct of the inactivated enzyme complex. When the enzyme was denatured, the peak shifted to -114.3ppm (a 7.4 ppm shift downfield) and resolved into a doublet of doublets, coupled with the two adjacent protons. This suggests that the fluorine is more shielded in the enzyme pocket, likely the effect of weak electrostatic fields,³⁹ which has been observed in other fluorinated protein ¹⁹F NMR studies. The change in the fluorine splitting is attributable to a broadening 40 in the peak due to the chemical shielding anisotropy contribution to the relaxation time of the nuclei. Collectively, these spectra suggest that an inactivated adduct bearing a single fluorine atom is the most consistent structure from inactivation of hOAT by 5. A fluorine atom was present in the active site, which was released upon denaturation, suggesting it was part of the PLP/inactivator complex. This indicates that pathway a, in which rapid aromatization occurs after the second deprotonation step, is most plausible.

To further confirm these results, a sample of hOAT inactivated by 5 was denatured and the released small molecules were analyzed using LC-HRMS with alternating positive and negative mode electrospray to determine the molecular mass of the released PLP-5 complex. The major mass peak, observed in the correct range, was consistent with the PLP-5 adduct containing a single fluorine atom (obs: 387.0746, theoretical: 387.0752) (Figure S11). The isotopic abundance of the parent ion as well as the spectra of MS/MS were consistent with elimination of one fluoride ion and rapid aromatization to give the PLP-5 adduct, further supporting inactivation pathway a, and eliminating pathway c.

As seen in the crystal structure (Figure 3), the remaining fluorine atom on the inactivator (the green atom) forms hydrophobic-like interactions with the side chain carbons of Glu235, aiding in the tight binding of the inactivator—PLP complex in the active site of hOAT. Although fluorine is able to form hydrogen bonds, there are no active site residues that reside within hydrogen bonding distance to the single fluorine atom of the inactivating adduct. Additionally, Tyr85 and Phe177 stabilize the pose of the inactivator aromatic ring, thus contributing to molecular recognition (Figure 4).

Determination of the Turnover Mechanism to Metabolites. The partition ratio of an MBI is the number of turnovers of the compound acting as an alternate substrate per inactivation event per active site. Ideally, plotting the enzyme activity remaining after inactivation versus equivalents of compound added will provide a linear line from 100 to 0% enzyme activity remaining. The x-intercept of this line is the turnover number, or the number of inactivator molecules consumed per inactivation of a single enzyme active site. This turnover number represents the molecules turned over to ketone product and PMP plus the molecule that caused inactivation. As a result, the partition ratio is the turnover number minus one (based on the established 1:1 stoichiometry

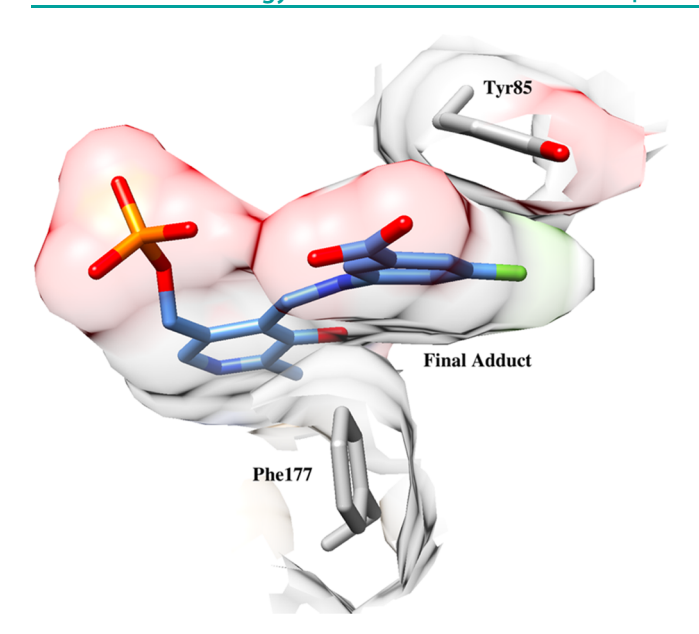


Figure 4. Final adduct displayed with the inactivator bound to PLP and Tyr85 and Phe177 closely contouring the complex. The surface feature distinguishes the van der Waals surface of each residue.

of inactivator to enzyme in the inactivated complex). The turnover number for **5** was determined to be 2.2 by titrating a fixed amount of *h*OAT with varying equivalents of **5**, measuring the remaining enzyme activities for the different equivalents of inhibitor, and employing the method of Pham et al.⁴² (Figure S12). The partition ratio, therefore, is 1.2. The nonlinear part of the graph indicates deviation from pseudofirst order inactivation kinetics at higher concentrations of **5**, and probably represents competition of the product with **5** for the active site.⁴³ A similar effect was observed in the inhibition of GABA-AT by the previously reported inactivator CPP-115.⁴⁴

To identify turnover products produced during the inactivation of hOAT by **5**, a sample of hOAT was inactivated in the presence of $\alpha\text{-KG}$, which facilitates multiple turnover cycles and maximizes the yield of the turnover products. The sample was then filtered through a 10 kDa molecular weight cutoff spin filter to remove the protein. The flowthrough was collected, and the sample was then subjected to untargeted LC-HRMS with alternating positive and negative mode electrospray. Three possible turnover products were proposed, **34**, **35**, and **36** (Figure **5**). Among the potential metabolites,

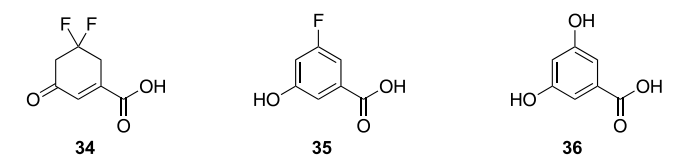


Figure 5. Potential metabolites.

34 was detected (observed 177.1108 m/z, [M + H]⁺; theoretical: 177.0358 m/z), and tandem mass spectrometry (MS/MS) showed fragmentation consistent with 34 (Figure 6).

In addition to mass spectrometry, UV—vis spectrophotometry (Figure 7) was utilized as a qualitative/confirmatory method to gather evidence for PMP formation resulting from turnover of the inactivator. An initial spectrum of the hOAT

was collected (black), displaying a peak at 420 nm indicative of an internal aldimine. The enzyme was then treated with 1 mM of 5, and another spectrum was collected after 2 min (red). The decay of internal aldimine absorption peak at 420 nm with concomitant formation of a peak at 330 nm was observed. If PMP is produced upon turnover of the inactivator, the addition of α -KG is expected to result in reformation of a peak within the 410-420 nm range, characteristic of the PLP form of the cofactor. After hOAT was incubated with 5 for 4 min, 1 mM α -KG was added to the sample, and a third spectrum was immediately recorded (green). The observed reformation of a peak at 415 nm is indicative of transient accumulation of the external aldimine intermediate, assuming the binding of 5 is rapid; this observation further supports that PMP is likely produced upon turnover of 5 by hOAT. Two minutes after α -KG addition, a fourth spectrum was collected (blue). The peak at 415 nm decayed, presumably resulted from the subsequent engagement of residual 5 inactivating the PLP form of hOAT generated by the addition of α -KG. The steady accumulation at 330 nm is most likely a combination of the absorbance from PMP production and the final adduct of the inactivated enzyme.

Transient State Measurements of hOAT Inactivation by 5. The data collected using stopped-flow spectrophotometry serves as additional evidence for the proposed mechanism. As can be seen from the inset in Figure 8, the extracted traces at each wavelength are ostensibly mirror images of each other and fit to return the same observed rate constant within error, indicating that there is likely only one phase that is observable spectrophotometrically. This single phase includes the near-complete loss of the peak at 420 nm and the generation of a new peak at 325 nm. As shown above, the peak at 420 nm is present in the native enzyme and is common to enzymes containing the PLP cofactor. Diminishment of this peak is assigned as the loss of PLP as the initial adduct is formed. As described above, there are two possible explanations for the peak at 325 nm: formation of the final adduct and formation of PMP resulting from the deamination of 5. It has been shown that the addition of α -KG after an initial incubation period with 5 causes a temporary partial regeneration of the peak at 420 nm but does not appreciably diminish the peak at 325 nm (Figure 8). This indicates that the absorbance at 325 nm arises primarily from the final adduct instead of PMP; however, the absorbance at this wavelength likely contains contributions from both species.

These spectrophotometric data indicate that the rate-limiting step of the processes is the same in the turnover and inactivation mechanisms, consistent with the idea that γ -proton abstraction from the initial external aldimine is rate-limiting. The subsequent increase in absorbance at 325 nm would thus report the accumulation of both the turnover and inhibition products, with no difference in rates. In the absence of more spectrophotometric signals, it is impossible to assign intrinsic rates of specific steps; however, the dependence of the observed rate of decay accumulation of the absorption at 325 nm has a hyperbolic dependence, indicating that the dissociation constant for reversible formation of the external aldimine is 2.9 \pm 0.4 mM, consistent with 5 being a relatively bulky non-native ligand.

DISCUSSION

Plausible Mechanisms for 5. Based on all obtained results, the plausible inactivation mechanism is shown in

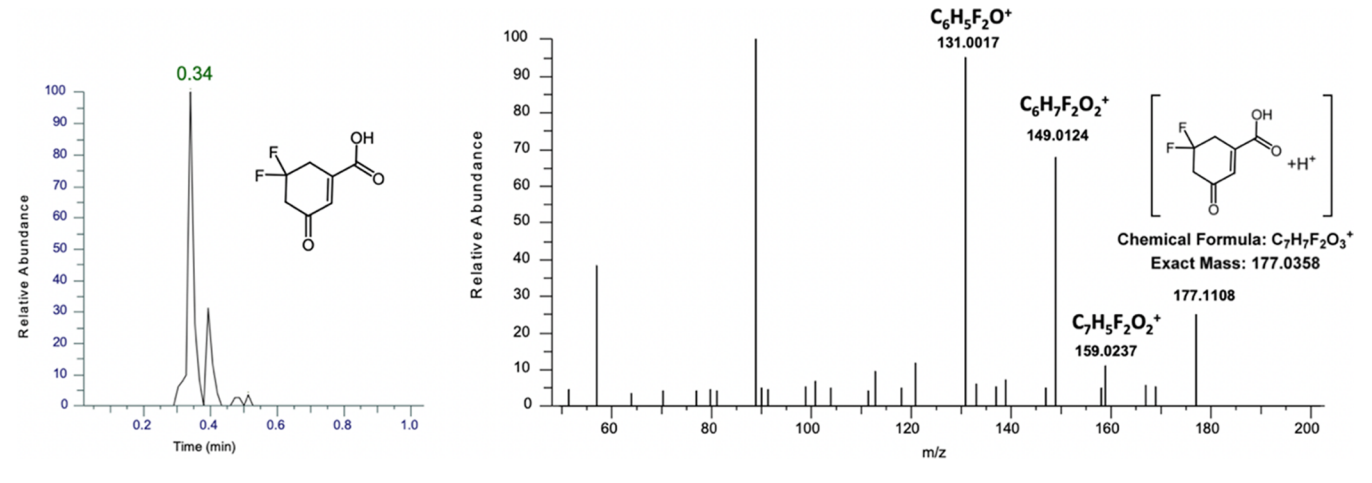


Figure 6. Small-molecule mass spectrometry analysis of metabolites.

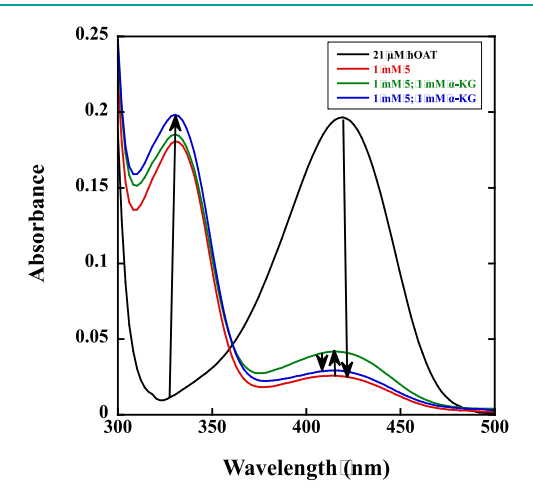


Figure 7. UV—vis spectra of hOAT with 5 and α -KG. Arrows indicate the sequence of the observed spectra after initiating the experiment. The decay of the external aldimine intermediate (red), transient accumulation of the external aldimine intermediate (green), and subsequent turnover and decay of the external aldimine intermediate (blue) are displayed.

Scheme 6, which commences with the condensation of inactivator 5 with Lys292-PLP complex 6, displacing the lysine and producing the external aldimine intermediate (7). Intermediate 7 is then deprotonated by Lys292 at the γ position, followed by a rapid tautomerization to quinonoid intermediate 8, resulting in the formation of the ketimine intermediate (9). A second deprotonation by Lys292 at the δ position of 9 produces activated intermediate 10, which rapidly aromatizes to the final tight-binding adduct (11). This is the structure that was captured in the crystal structure of the inactivated enzyme (Figure 3). Based on the turnover number/ partition ratio study (Figure S12), turnover results in inactivation 45% of the time (once for three turnovers). In addition to the inactivation pathway, 45% of 5 undergoes turnover to a product, 34 and PMP. The structure of the turnover product was supported by LC-MS and confirmed by its fragmentation spectrum (Figure 6). The use of UV-vis spectrophotometry confirmed PMP production upon turnover of the inactivator (Figure 7).

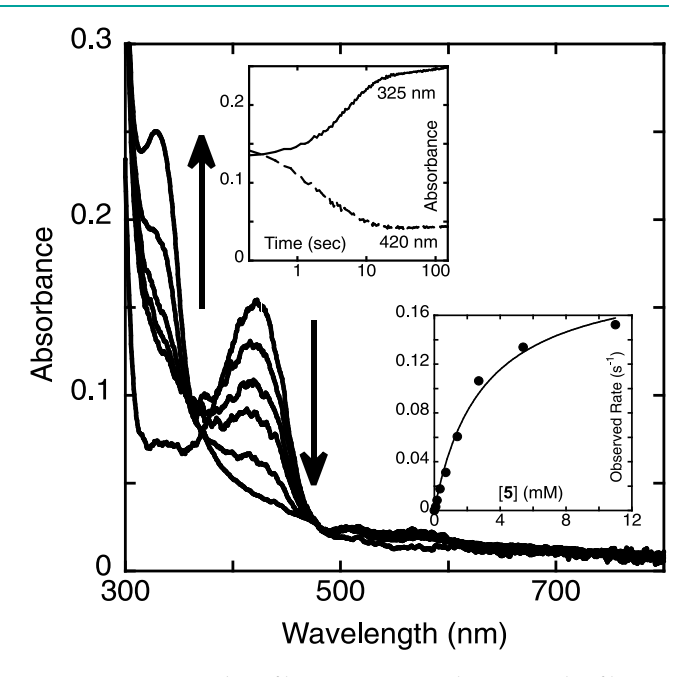


Figure 8. Kinetic studies of hOAT reacting with 5. A sample of hOAT (17 μ M) was mixed with 5 (0–11 mM) using a stopped-flow spectrophotometer, and the reaction was observed between 300 and 800 nm for 150 s using CCD detection. Several representative spectra from the data set are shown here. The top inset plot depicts the change in absorbance at the two peak maxima, 325 and 420 nm, with respect to time. These data were fit to a single-step irreversible model using SVD. The lower inset depicts the dependence of observed rate constants on the concentration of [5]. Fitting to a rectangular hyperbolic function ($k_{\rm obs} = k_{\rm limit}[5]/K_{[5]}+[5]$) returned an observed limiting rate constant of 0.20 \pm 0.01 s⁻¹ and a dissociation constant for reversible formation of the external aldimine of 2.9 \pm 0.4 mM.

CONCLUSIONS

In recent years, the selective inactivation of human ornithine aminotransferase (hOAT) has been of significant interest as a potential therapeutic approach to halt the progression of hepatocellular carcinoma (HCC).²⁹ A recent advance in the efforts to improve the potency and selectivity of mechanism-based inactivators of hOAT over other aminotransferase enzymes involved expanding the cyclopentene scaffold previously developed for γ -aminobutyric acid aminotransferase

Scheme 6. Plausible Mechanism of Inactivation of hOAT by 5

(GABA-AT) inactivators into a series of cyclohexene analogues. Previous cyclohexene inactivators reported have shown improved selectivity for hOAT over GABA-AT, likely due to their increased sizes being better accommodated in the active site of hOAT. In this work, a novel series of fluorinated cyclohexene analogues was rationally designed, synthesized, and evaluated for the inactivation of hOAT. Of the potential inactivators, 5 was demonstrated to be a selective inactivator of hOAT, resulting in a tight-binding adduct. A plausible mechanism of inactivation of hOAT by 5 is proposed (Scheme 6), which was elucidated using a variety of experimental methods, including X-ray crystallography, ¹⁹F NMR spectroscopy, mass spectrometry, and stopped-flow spectrophotometry. A previous study on the mechanism of inactivation of hOAT by (S)-3-amino-4,4-difluorocyclohex-1-ene-1-carboxylic acid concluded that, for this MBI, nucleophilic attack by Lys292 leads to the formation of a ternary final adduct.³³ Interestingly, in the inactivation mechanism of 5 with hOAT, despite the enhanced electrophilicity at C_{ε} of 10 conferred by the remaining fluorine atom, Lys292 did not attack the inactivator-PLP complex to form a ternary adduct. In the binding pocket, the position of the electrophilic center at C_{ε} is observed as distal from Lys292, likely accounting for the lack of

Lys292 nucleophilic attack on 10. In addition, although structural evidence indicates the inactivated adduct is solvent-accessible (Figure S13), no water molecule was involved in the inactivation mechanism of hOAT, only the turnover mechanism. We believe this may be due to the lack of active site residues proximal to C_{ε} that could activate and assist water molecules for nucleophilic attack. This differs from the inactivation mechanisms of GABA-AT by previously reported potent inactivators CPP-115⁴⁴ and vigabatrin and emphasizes the critical role of active site differences between hOAT and GABA-AT. Collectively, these findings provide insight into the future rational design of mechanism-based inactivators of hOAT.

■ EXPERIMENTAL SECTION

General Synthetic Methods. All chemicals were purchased from Sigma-Aldrich, Acros Organics, Fisher Scientific, or Combi-blocks and used without further purification. Anhydrous solvents (THF, CH₃CN, DMF) were purified before use by passing through a column composed of activated alumina and a supported copper redox catalyst. Yields refer to chromatographically homogeneous materials. Flash column chromatography was performed on a Teledyne Combiflash Rf Plus automated flash purification system with various Teledyne cartridges (4–80 g, 40–63 μm, 60 Å). Purifications were performed

with hexanes and ethyl acetate unless otherwise noted. Preparatory column chromatography was performed on a Teledyne ACCQPrep HP150 using a Phenomenex Luna Omega Polar C18 preparatory HPLC column (150 mm \times 21.2 mm, 5 μ m) with water/MeCN with 0.1% formic acid as the solvent system. ¹H and ¹³C NMR spectra were recorded on a Bruker Avance III NMR spectrometer at 500 and 126 MHz, respectively, in CDCl₃, CD₃OD, or DMSO-d6. ¹⁹F NMR spectra were recorded on a 400 MHz Bruker Avance III HD Nanobay system. Chemical shifts were reported in ppm; multiplicities are indicated by s = singlet, brs = broad singlet, d = doublet, t = triplet, q= quartet, dd = doublet of doublet, dt = doublet of triplet, dq = doublet of quartet, m = multiplet resonance. Coupling constants "J" were reported in Hz. High-resolution mass spectral data were obtained on an Agilent 6210 LC-TOF spectrometer in the positive ion mode using electrospray ionization with an Agilent G1312A HPLC pump and an Agilent G1367B autoinjector at the Integrated Molecular Structure Education and Research Center (IMSERC), Northwestern University. Analytical HPLC was performed using a reversed-phase Agilent Infinity 1260 HPLC with a Phenomenex Kintex C18 column (50 mm \times 2.1 mm, 2.6 μ m), detecting with UV absorbance at 254 nm. All final products were shown to be >95% pure by HPLC.

Compound 17 was prepared in accordance with literature procedures. 35,36

N-((1R,3S,4R,5R)-4-Bromo-7-oxo-6-oxabicyclo[3.2.1]octan-3-yl)acetamide (18). To a stirred solution of N-bromoacetamide (4.0 g, 29.00 mmol, 1.2 equiv) in dry CH₃CN (100 mL) in the dark were added SnCl₄ (1 M in DCM, 9.67 mL, 9.67 mmol, 0.4 equiv) and water (0.522 mL, 29.00 mmol, 1.2 equiv) at r.t. After 5 min, to this solution was added 17 (3.0 g, 24.17 mmol, 1.0 equiv) in dry CH₃CN (20 mL). The reaction was stirred at r.t. overnight in the dark. After the completion of the reaction was indicated by TLC (hexane:EtOAc = 2:1), the reaction was quenched with aqueous Na₂SO₃ (50 mL) and aqueous NaHCO₃ (50 mL). The mixture was extracted with DCM (150 mL) 3 times. The organic phase was separated, combined, washed with brine (150 mL), and dried with anhydrous Na₂SO₄. The solution was concentrated and diluted with EtOAc (30 mL). The suspension was stirred at r.t. for 2 h before the filtration. The white solid was collected and dried (18, 4.235 g, 67%). ¹H NMR (500 MHz, CDCl₃) δ 6.09 (d, J = 4.8 Hz, 1H), 4.91 (dd, J = 5.8, 4.0 Hz, 1H), 4.59 (t, J = 7.2 Hz, 1H), 4.26 (dd, J = 3.7, 1.3 Hz, 1H), 2.68-2.64 (m, 2H), 2.39 (ddd, J = 14.7, 6.6, 2.9 Hz, 2H), 2.02 (dtd, J = 14.7), 214.7, 3.7, 1.7 Hz, 1H), 1.95 (s, 3H). 13 C NMR (126 MHz, CDCl₃) δ 178.6, 169.2, 79.5, 50.1, 45.9, 35.8, 31.9, 30.1, 23.3. LRMS [M + H]⁺: 261.9, calcd for $C_9H_{13}BrNO_3$ (M + H⁺): 262.0.

N-((1R,3S,5R)-7-Oxo-6-oxabicyclo[3.2.1]octan-3-yl)acetamide (19). To a solution of 18 (25.05 g, 95.6 mmol, 1.0 equiv) in benzene (774 mL) were added AIBN (1.57 g, 9.6 mmol, 0.1 equiv) and Bu₃SnH (30.9 mL, 114.7 mmol, 1.2 equiv). The solution was degassed and then refluxed for 12 h. The solution was allowed to cool to RT before being concentrated under reduced pressure. To the resulting oil was added diethyl ether (200 mL), and the resulting solution was stirred for an hour during which time a white solid formed. The solution was filtered and the precipitate was washed with diethyl ether. The resulting white solid was purified by silica gel chromatography (0-30% MeOH in DCM) to afford 19 as a white solid (14.7 g, 84% yield). 1 H NMR (500 MHz, CDCl₃) δ 6.07 (s, 1H), 4.93-4.87 (m, 1H) 4.43-4.36 (m, 1H), 2.59 (q, J = 4.3, 3.8 Hz, 1H), 2.46 (dt, J = 11.5, 5.4 Hz, 1H), 2.18 (d, J = 13.4 Hz, 1H), 2.04 (dd, J = 4.3, 2.2 Hz, 2H), 1.96 (ddd, J = 14.5, 6.1, 2.8 Hz, 1H), 1.90 (s, 3H), 1.79 (d, J = 11.7 Hz, 1H). ¹³C NMR (126 MHz, CDCl₃) δ 179.29, 169.35, 77.48, 42.31, 36.84, 36.15, 33.70, 33.56, 23.46. HRMS (ESI) calcd for C₉H₁₃NO₃Na (M+Na⁺): 206.0793, found: 206.0792.

Methyl (1R,3S,5R)-3-Acetamido-5-hydroxycyclohexane-1-carboxylate (20). To 19 (8.6 g, 46.8 mmol, 1 equiv) at 0 °C was added 3.0 M HCl in methanol (40 mL) slowly. The resulting solution was then heated to 40 °C and stirred for 18 h until the starting material was consumed by LC-MS. The reaction was concentrated to afford 20 as a white solid (10.1 g, 100%). ¹H NMR (500 MHz, Methanol- d_4) δ 3.72 (tt, J = 12.1, 3.9 Hz, 1H), 3.60 (s, 3H), 3.56 (dt,

J = 11.1, 4.2 Hz, 1H), 2.43 (tt, J = 12.7, 3.5 Hz, 1H), 2.13–1.98 (m, 3H), 1.95 (s, 3H), 1.23–1.07 (m, 3H). 13 C NMR (126 MHz, MeOD) δ 174.75, 174.72, 67.11, 51.00, 48.45, 39.93, 39.00, 36.59, 33.28, 20.31. HRMS (ESI) calcd for C₁₀H₁₇NO₄Na (M+Na⁺): 238.1055, found: 238.1050.

Methyl (1R,3S)-3-Acetamido-5-oxocyclohexane-1-carboxylate (21). To a solution of 20 (2.4 g, 11.4 mmol) in DCM (80 mL) was added PCC (7.3 g, 34.2 mmol, 3.0 equiv). The resulting solution was stirred overnight at RT. Upon completion, the reaction was quenched by the addition of 30 mL sat. aq. Na₂S₂O₃ and stirred for an hour until the brown solution turned a light green. The reaction was then filtered and acidified with 1 M HCl (4 mL). This mixture was diluted with EtOAc, and the organic layer was collected. The aqueous layer was extracted with EtOAc (6×40 mL). The organic layers were combined and washed with saturated brine (50 mL) and dried over Na₂SO₄, filtered, and concentrated to afford 21 as a white solid (1.6 g, 65%). ¹H NMR (500 MHz, CDCl₃) δ 4.21 (dtd, J = 11.4, 7.2, 3.9 Hz, 1H), 3.72 (s, 3H), 2.88-2.79 (m, 1H), 2.79-2.70 (m, 1H), 2.63 (ddt, J = 14.9, 4.9, 1.7 Hz, 1H), 2.55–2.38 (m, 2H), 2.25 (ddd, J = 14.4, 11.5, 1.1 Hz, 1H), 1.99 (s, 3H), 1.75 (dt, J = 13.1, 11.2 Hz, 1H). ¹³C NMR (126 MHz, CDCl₃) δ 205.6, 173.8, 169.4, 52.4, 47.0, 46.9, 42.4, 39.3, 33.8, 23.4. LRMS [M + H]+: 214.2, calcd for C₁₀H₁₆NO₄ (M + H⁺): 214.2.

Methyl (1R,5S)-5-Acetamido-3,3-difluorocyclohexane-1-carboxylate (22) and Methyl (1S,5R)-5-Acetamido-3-fluorocyclohex-3-ene-1-carboxylate (23). To a solution of 21 (2.7 g, 13.1 mmol, 1.0 equiv) in DCM (80 mL) in a plastic RBG was added DAST (5.0 mL, 38.0 mmol, 3.0 equiv) at 0 °C. The solution was allowed to warm to room temp and then heated to 50 °C for 5 h. The reaction was then allowed to cool to RT and was quenched by the addition of 20 mL sat. aq. NaHCO₃. This mixture was diluted with DCM, and the organic layer was collected. The aqueous layer was extracted with DCM (2 \times 20 mL). The organic layers were combined and washed with saturated brine (20 mL) and dried over Na₂SO₄, filtered, and concentrated. The resulting residue was purified by silica gel chromatography (0–100% EtOAc in hexane) to afford a mixture of 22 and 23 as a white solid (2.31 g) which was carried forward without further purification.

Methyl (5S)-3,3-Difluoro-5-(2,2,2-trifluoroacetamido)cyclohexane-1-carboxylate (24). To a 40 mL vial equipped with a pressure relief lid were added a mixture of 22 and 23 (3.21 g, \sim 13 mmol, 1.0 equiv) followed by 60 mL of 3 M HCl in methanol. The vial was heated to 75 °C for 2 days. After which, the solution was allowed to cool to RT, concentrated, and azeotroped with toluene. The residue was then suspended in DCM (20 mL) and TFAA (3 mL) and stirred overnight at RT. The reaction was then concentrated, and the resulting residue was purified by silica gel chromatography (0-40% EtOAc in hexane) to afford 23 as a white solid (945 mg, 25% from 21). ¹H NMR (500 MHz, CDCl₃) δ 6.63 (s, 1H), 4.18 (tdt, J =11.5, 8.6, 4.4 Hz, 1H), 3.73 (s, 3H), 2.81 (tt, J = 11.1, 4.2 Hz, 1H), 2.50-2.30 (m, 3H), 2.06-1.76 (m, 2H), 1.59 (q, J = 12.2 Hz, 1H). ^{13}C NMR (126 MHz, CDCl₃) δ 173.42, 156.54 (d, J = 37.4 Hz), 124.90-119.41 (m), 115.59 (d, J = 287.9 Hz), 52.53, 45.44 (d, J =10.1 Hz), 38.50 (t, J = 24.6 Hz), 37.55 (d, J = 9.4 Hz), 35.30 (t, J = 10.1 Hz) 25.0 Hz), 32.14. HRMS (ESI) calcd for C₁₀H₁₁F₅NO₃ (M - H): 288.0659, found: 288.0665.

Methyl (S)-3,3-Difluoro-5-(2,2,2-trifluoroacetamido)cyclohex-1-ene-1-carboxylate (26) and Methyl (R)-5,5-Difluoro-3-(2,2,2-trifluoroacetamido)cyclohex-1-ene-1-carboxylate (25). To a solution of 1 M KHMDS (7.85 mL, 7.85 mmol, 2.4 equiv) in dry THF (10 mL) at $-78~^{\circ}\mathrm{C}$ was added a solution of 24 (945 mg, 3.3 mmol, 1.0 equiv) in THF dropwise over 20 min. The solution was stirred for 3 h at $-78~^{\circ}\mathrm{C}$, after which a solution of PhSeBr (900 mg, 2.0 mmol, 1.4 equiv) in THF was added. The reaction was allowed to warm to RT overnight, after which it was quenched by the addition of 15 mL of sat. aq. NH₄Cl. This mixture was diluted with EtOAc, and the organic layer was collected. The aqueous layer was extracted with EtOAc (2 \times 10 mL). The organic layers were combined and washed with saturated brine 105 mL and dried over Na₂SO₄, filtered, and concentrated. The resulting residue was purified by silica gel plug (0–

100% EtOAc in hexane), and the resulting light yellow oil was carried on crude.

To a solution of the yellow oil in DCM (5 mL) was added mCPBA (820 mg, 3.3 mmol, 1.5 equiv), and the reaction was stirred for 3 h at RT. The reaction was quenched by the addition of 10 mL sat. aq. Na₂S₂O₃ and diluted with DCM, and the organic layer was collected. The aqueous layer was extracted with DCM (2 \times 10 mL). The organic layers were combined and washed with sat. aq. NaHCO₃ (10 mL), saturated brine (10 mL), and dried over Na₂SO₄, filtered, and concentrated. The resulting residue was purified by silica gel plug (0-20% MeOH in DCM), to provide a 1:1 mixture of 26 and 25 (534.5 mg, 56% over two steps). Purification by C18 silica gel chromatography (10-90% MeCN in water) 26 (230 mg, 24.5% over two steps) and 25 (220 mg, 23.4% over two steps) as white solids along with mixed fractions. Both 25 and 26 were recrystallized by slow diffusion of hexanes into diethyl ether at 4 °C to obtain single-crystal X-ray structures to confirm the absolute stereochemistry. **26**: ¹H NMR (500 MHz, CDCl₃) δ 6.84 (td, I = 5.2, 2.5 Hz, 1H), 6.50 (s, 1H), 4.45 (dq, J = 11.7, 5.6 Hz, 1H), 3.81 (s, 3H), 2.81 (dqd, J = 18.0, 4.9, 2.0 Hz, 1H), 2.55-2.36 (m, 2H), 2.30 (qd, J = 13.3, 8.5)Hz, 1H). HRMS (ESI) calcd for $C_{10}H_9F_5NO_3$ (M – H): 286.0502, found: 286.0514.

25: ¹H NMR (500 MHz, CDCl₃) δ 6.85 (dt, J = 4.3, 2.0 Hz, 1H), 6.48 (d, J = 8.0 Hz, 1H), 5.03 (s, 1H), 3.79 (s, 3H), 2.96 (dddd, J = 18.5, 12.4, 10.5, 1.8 Hz, 1H), 2.83–2.69 (m, 1H), 2.44–2.30 (m, 1H). HRMS (ESI) calcd for $C_{10}H_9F_5NO_3$ (M - H): 286.0502, found: 286.0509.

(R)-3-Amino-5,5-difluorocyclohex-1-ene-1-carboxylic Acid Hydrochloride (5). To a 40 mL vial equipped with a pressure relief lid were added 26 (215 mg, 0.75 mmol) and 4 M HCl aq at 80 C until the starting material and monodeprotected intermediates were consumed. The reaction was then concentrated and azeotropde with acetonitrile (3 × 20 mL). The material was purified via a C18 aqueous column (0–40% MeCN in water) to yield 5 as a tan solid (70.4 mg, 43% yield). ¹H NMR (500 MHz, D₂O) δ 6.83 (s, 1H), 4.34 (d, J = 7.6 Hz, 1H), 2.97–2.80 (m, 2H), 2.59 (ddt, J = 19.9, 12.9, 6.0 Hz, 1H), 2.31–2.17 (m, 1H). ¹³C NMR (126 MHz, D₂O) δ 168.42, 131.81, 131.01, 121.70 (d, J = 239.2 Hz), 46.03, 33.18–32.63 (m). ¹⁹F NMR (470 MHz, D₂O) δ –93.69 (d, J = 247.2 Hz), -95.90 (d, J = 247.1 Hz). HRMS (ESI) calcd for $C_7H_{10}F_2NO_2$ (M + H⁺): 178.0679, found: 178.0673.

(*S*)-5-Amino-3,3-difluorocyclohex-1-ene-1-carboxylic Acid Hydrochloride (*4*). 4 was prepared from **25** (50 mg, 0.18 mmol) via the same procedure as **5**. 4 was isolated as a tan solid (33 mg, 87% yield) Characterization: 1 H NMR (500 MHz, D₂O) δ 6.96–6.85 (m, 1H), 3.92 (tt, J = 9.1, 4.1 Hz, 1H), 3.04 (dd, J = 18.2, 6.2 Hz, 1H), 2.77 (tdt, J = 13.1, 8.6, 4.3 Hz, 1H), 2.60 (ddt, J = 17.9, 9.1, 2.9 Hz, 1H), 2.47 (dddd, J = 22.5, 13.7, 11.1, 9.2 Hz, 1H). 13 C NMR (126 MHz, D₂O) δ 168.40, 136.09 (t, J = 10.5 Hz), 127.75 (dd, J = 31.6, 28.4 Hz), 117.86 (t, J = 233.1 Hz), 43.55 (d, J = 8.1 Hz), 34.11 (t, J = 25.7 Hz), 27.31. 13C NMR (126 MHz, D₂O) δ 168.40, 136.09 (t, J = 10.5 Hz), 127.75 (dd, J = 31.6, 28.4 Hz), 117.86 (t, J = 233.1 Hz), 43.55 (d, J = 8.1 Hz), 34.11 (t, J = 25.7 Hz), 27.31, 20.41. 19F NMR (470 MHz, D₂O) δ -83.62 - -86.13 (m), -91.33 (dq, J = 284.2, 9.0 Hz). HRMS (ESI) calcd for C₇H₁₀F₂NO₂ (M + H $^+$): 178.0679, found: 178.0681.

Methyl cis-3-((tert-Butoxycarbonyl)amino)-5-hydroxycyclohexane-1-carboxylate (28). To a stirred solution of 3-amino-5-hydroxybenzoic acid hydrochloride (27) (4.0 g, 21.1 mmol, 1.0 equiv) in water (10 mL) was added Rh/Al₂O₃ (15 wt %, 150 mg). The suspension was charged with high-pressure H₂ (400 psi), heated to 90 °C, and stirred overnight. After the completion of reaction was detected by LC-MS, the suspension was filtered. The obtained filtrate was concentrated and then diluted with MeOH (20 mL). The solution was cooled to 0 °C with an ice bath, followed by slow addition of SOCl₂ (4.65 mL, 63.29 mmol, 3.0 equiv) under Ar. The solution was warmed to r.t. and stirred for 1 h. After the completion of reaction was detected by LC-MS, the solution was concentrated and diluted with MeOH (20 mL). To this stirred solution were added Boc₂O (6.91 g, 31.65 mmol, 1.5 equiv) and NaHCO₃ (5.32 g, 63.29

mmol, 3.0 equiv). The suspension was stirred at r.t. overnight before being filtered. The filtrate was concentrated and purified by silica gel chromatography (50–100% EtOAc in hexane) to afford a white solid (28, 2.13 g, 37%). $^1\mathrm{H}$ NMR (500 MHz, CDCl₃) δ 4.54 (brs, 1H), 3.76–3.69 (m, 1H), 3.68 (s, 3H), 3.59–3.48 (m, 1H), 2.43 (tt, J = 12.2, 3.6 Hz, 1H), 2.28–2.15 (m, 3H), 1.86 (d, J = 4.5 Hz, 1H), 1.43 (s, 9H), 1.37 (q, J = 12.3 Hz, 1H), 1.23 (q, J = 12.2 Hz, 1H), 1.13 (q, J = 11.4 Hz, 1H). $^{13}\mathrm{C}$ NMR (126 MHz, CDCl₃) δ 174.8, 155.2, 79.7, 68.3, 52.1, 47.2, 41.7, 39.3, 37.0, 34.8, 28.5. LRMS [M + H]*: 274.0, calcd for $\mathrm{C_{13}H_{24}NO_5}$ (M + H*): 274.2.

Methyl cis-3-((tert-Butoxycarbonyl)amino)-5-oxocyclohexane-1-carboxylate (29). To a stirred solution of 28 (2.13 g, 7.79 mmol, 1.0 equiv) in DCM (100 mL) was added PCC (5.04 g, 23.38 mmol, 3.0 equiv). The suspension was stirred at r.t. overnight. The reaction was filtered, and the obtained filtrate was concentrated and purified by silica gel chromatography (0–20% EtOAc in DCM) to afford a white solid (29, 1.68 g, 80%). 1 H NMR (500 MHz, CDCl₃) δ 4.58 (brs, 1H), 3.84 (brs, 1H), 3.71 (s, 3H), 2.78–2.69 (m, 2H), 2.59 (ddt, J = 14.9, 4.6, 1.8 Hz, 1H), 2.51–2.43 (m, 2H), 2.28–2.16 (m, 1H), 1.79–1.66 (m, 1H), 1.44 (s, 9H). 13 C NMR (126 MHz, CDCl₃) δ 205.9, 173.8, 154.7, 80.1, 52.5, 48.3, 47.7, 42.6, 39.4, 34.7, 28.5. LRMS [M + H]*: 272.1, calcd for $C_{13}H_{22}NO_5$ (M + H*): 272.1.

Methyl cis-5-((tert-Butoxycarbonyl)amino)-3,3-difluorocyclohexane-1-carboxylate (30). To a stirred solution of 29 (700 mg, 2.58 mmol, 1.0 equiv) in 1,2-dichloroethane (30 mL) was added DAST (1.36 mL, 10.32 mmol, 3.0 equiv). The solution was heated to 40 $^{\circ}$ C and stirred overnight. The completion of the reaction was indicated by TLC (hexane:EtOAc = 2:1). The reaction was quenched with aqueous NaHCO3 (20 mL) and extracted with DCM (30 mL) 3 times. The organic phase was separated, combined, washed with brine (50 mL), and dried with anhydrous Na₂SO₄. The solution was concentrated and purified by silica gel chromatography (0-10% EtOAc in hexane) to afford a white solid (30, 448 mg, 59%). ¹H NMR (500 MHz, CDCl₃) δ 4.46 (s, 1H), 3.77 (s, 1H), 3.70 (s, 3H), 2.68 (ttd, J = 12.8, 3.8, 1.6 Hz, 1H), 2.49-2.30 (m, 3H), 1.80 (dtd, J= 34.2, 13.4, 3.3 Hz, 1H), 1.44 (s, 10H), 1.29 (q, J = 12.6 Hz, 1H). 13 C NMR (126 MHz, CDCl₃) δ 173.4, 154.7, 122.2 (dd, J = 244.1, 239.2 Hz), 79.9, 52.2, 46.0, 40.0 (t, J = 23.7 Hz), 37.8 (d, J = 10.8Hz), 35.5 (t, J = 25.1 Hz), 34.3 (d, J = 1.6 Hz), 28.3. LRMS [M + H]⁺: 294.0, calcd for $C_{13}H_{23}F_2NO_4$ (M + H⁺): 294.1.

cis-5-Amino-3,3-difluorocyclohexane-1-carboxylic Acid Hydrochloride (*3*). Following the same procedure as 5, 30 (50 mg) was converted to 3 (21 mg, 59%) as a white solid. ¹H NMR (500 MHz, CD₃OD) δ 3.41 (tt, J = 12.1, 4.3 Hz, 1H), 2.73 (ttd, J = 12.9, 3.8, 1.7 Hz, 1H), 2.52–2.35 (m, 3H), 1.99–1.83 (m, 2H), 1.57 (q, J = 12.5 Hz, 1H). ¹³C NMR (126 MHz, CD₃OD) δ 173.9 (d, J = 1.6 Hz), 121.6 (dd, J = 243.7, 238.2 Hz), 46.3 (d, J = 11.9 Hz), 37.0 (dd, J = 16.4, 6.2 Hz), 36.8 (d, J = 25.6 Hz), 34.7 (t, J = 24.7 Hz), 30.9 (d, J = 1.4 Hz). HRMS (ESI) (m/z) [M - M] calcd for C₇H₁₀F₂NO₂ = 178.0685, found = 178.0686.

Expression and Purification of hOAT. The expression and purification of hOAT were performed similarly to previously published protocols. 46 In brief, Escherichia coli BL21 (DE3) cells containing the pMAL-t-hOAT plasmid were incubated at 37 °C and shaken at 200 rpm in 1 L of Luria-Bertani (LB) medium containing 100 μ g/mL ampicillin. Upon reaching an OD₆₀₀ value of 0.7 absorbance units, the cell culture was incubated on ice for 60 min before induction. Expression of the MBP-t-OAT fusion protein was induced utilizing 400 μ M isopropyl β -D-1-thiogalactopyranoside, and the culture was incubated at 18 °C while being shaken at 200 rpm for 17 h. The cells were harvested by two periods of centrifugation at 12400g for 20 min before being resuspended in buffer A containing 50 mM Tris-HCl, 200 mM NaCl, and 100 μ M PLP, pH 7.4. The suspension was lysed with one 5 min period of sonication and followed by an additional two 20 min periods of centrifugation at 40,000g to pellet cell debris. The resulting supernatant was loaded onto an amylose affinity column pre-equilibrated with buffer A. The column was washed with 35 mL of buffer A before the MBP-t-OAT fusion protein was eluted utilizing a 100 mL linear gradient of buffer A supplemented with 10 mM maltose. Individual 4 mL fractions

containing the MBP-t-OAT fusion protein were combined. To remove the MBP tag, the protein sample was diluted to $\sim\!45$ mL with cleavage buffer containing 50 mM Tris, 100 mM NaCl, pH 8.0 and treated with tobacco etch virus protease for 12 h at 10 °C with 60 rpm agitation. Following cleavage, a 50,000 molecular weight cutoff (MWCO) Amicon Ultra centrifugal filter device was utilized to concentrate the protein mixture until the sample volume was less than 5 mL. For further purification, the sample was loaded onto a HiLoad Superdex-200PG column (16 mm \times 600 mm) pre-equilibrated with buffer A and subjected to size exclusion chromatography. The 4 mL fractions containing untagged $h{\rm OAT}$ were collected and quantified utilizing an extinction coefficient at 280 nm of 60200 ${\rm M}^{-1}$ cm $^{-1}$ and molecular weight of 48500 Da. Aliquots of $\sim\!1$ mg mL $^{-1}$ $h{\rm OAT}$ supplemented with 20% glycerol were frozen in liquid nitrogen and stored at -80 °C.

Expression and Purification of hGABA-AT and PYCR. Recombinant human brain γ -aminobutyric acid aminotransferase (hGABA-AT) was expressed and purified according to literature procedures with slight modifications. 26 Briefly, pelleted Expi293 cells were resuspended into buffer A containing 50 mM K₄O₇P₂ pH 8.6, 300 mM NaCl, and 100 μ M PLP. The suspension was lysed using four repeat cycles of sonication (10 s on, 10 s off, 20% amplitude) on ice followed by the addition of 12.5 mM MgCl, 125 μ M CaCl, and 5 mg of lyophilized DNase I. The lysate was incubated on ice for 60 min with periodic inversions followed by a two-step centrifugation procedure to pellet cell debris. Step 1 included centrifugation at 18000 rpm for 60 min at 4 °C followed by the collection of supernatant and a secondary step at 20000 rpm for 45 min. The supernatant was collected, and the sample was loaded into a disposable 0.45 μ m bottle-top vacuum filter system to remove remaining cell debris. The resulting sample was then loaded onto a Co²⁺-immobilized metal affinity chromatography column preequilibrated with buffer A. The column was washed with 40 mL of buffer A before hGABA-AT was eluted using a stepwise elution gradient of buffer A supplemented with 200 mM imidazole. The stepwise gradient totaled 5 steps of increasing imidazole concentration (1, 2, 5, 100, and 200 mM). Individual 4 mL fractions containing hGABA-AT were combined and concentrated to a volume of 3 mL using a 30000 Da molecular weight cutoff (MWCO) Amicon Ultra centrifugal filter device. For further purification, the sample was loaded onto a HiLoad Superdex-200PG column (16 mm × 600 mm) pre-equilibrated with buffer A and subjected to size exclusion chromatography at a flow rate of 0.25 mL/min. PYCR1 was purified according to previously published protocols.⁴⁷ Coupled enzyme assays for hGABA-AT, hOAT, Ala-AT, and Asp-AT were carried out according to previous procedures.²⁸

Dialysis Assay. The dialysis experiment was conducted using previous protocols. 26,47,28

Partition Ratio Experiment. The partition ratio was calculated using previous protocols. 26,47,28

¹⁹F NMR Spectroscopy Studies. After being fully inactivated by 5, a sample of hOAT was washed in distilled H₂O and diluted to 10 μ M and spiked with trifluoroethanol as an internal standard. The sample was run on a Bruker Neo 600 MHz system with a QCI (HFCN) Cryo Probe w/Z-Gradient at 298 K for 960 scans. Next, the same sample was denatured with the addition of 10 equiv of formic acid, and the resulting solution was heated to 55 °C for 10 min before being submitted to the same ¹⁹F NMR conditions.

Crystallization of hOAT Inactivated by 5, X-ray Data Collection and Processing, and Model Building and Refinement. Following confirmed inactivation of hOAT with 5, the sample was transferred to a 50,000 molecular weight cutoff (MWCO) Amicon Ultra centrifugal filter device and exchanged into buffer containing 100 mM Tricine, 100 mM NaCl, pH 7.8. The sample was then concentrated to \sim 6 mg mL $^{-1}$. Crystals were grown for 7 days at RT utilizing the hanging-drop vapor diffusion method with each drop initially containing 2 uL of inactivated hOAT and 2 uL of well solution. The crystals with the best morphology appeared in the well solution containing 10% PEG 6000, 100 mM NaCl, 20% glycerol, and 100 mM Tricine pH 7.8. Following 7 days of growth, hOAT crystals

with the best morphology were transferred into a cryo-protectant solution containing well solution supplemented with 30% glycerol prior to being frozen in liquid nitrogen. Monochromatic X-ray diffraction data were collected at the LS-CAT, Advanced Photon Source (APS), beamline 21-ID-D at Argonne National Laboratory (ANL, Argonne, IL). Data were collected at a wavelength of 1.127 Å and a temperature of 100 K using a Dectris Eiger 9 M detector. Data sets were processed and analyzed with autoPROC.⁴⁸ The structure of inactivated OAT was solved by molecular replacement utilizing PHASER⁴⁹ in Phenix.⁵⁰ The search model was the previously published structure of OAT (PDB code: 6 V8C). The model building and refinement were performed utilizing Coot⁵¹ and Phenix, respectively, until the lowest possible $R_{\rm free}/R_{\rm work}$ factor values were achieved. UCSF Chimera⁵² was used for the preparation of structural depiction figures. The structure factors and the refined model were deposited in the Protein Data Bank with PDB ID: 8 V9M.

UV–Vis Spectrophotometry. A Shimadzu UV-2450 spectrophotometer was utilized to collect absorbance spectra from 700 to 250 nm at 20 °C. The instrument was baselined with 1 mM 5 and 1 mM α -KG in reaction buffer containing 100 mM HEPES pH 7.5 and 200 mM NaCl. The initial concentration of hOAT was determined with A_{280} measurement and the molar extinction coefficient, previously calculated with amino acid composition.

Intact Protein Mass Spectrometry. The $h{\rm OAT}$ intact protein mass spectrometry samples were analyzed on an Orbitrap Eclipse (Thermo Fisher Scientific) mass spectrometer as previously reported. 47

Small-Molecule Mass Spectrometry. Samples were injected onto a Kinetex 1.3 µM, 100 Å C18 column on an Agilent 1290 Infinity II UHPLC system at 0.3 mL/min, in line with a Thermo Q-Exactive mass spectrometer at a monotonously increasing gradient of Solvent B (95% ACN/5% H2O/0.1%FA). Positive-mode ESI data were collected with the HESI source set to 3.6 kV, 10 sheath gas, 300 °C probe temperature, and 320 °C inlet capillary temperature. Untargeted data-dependent and targeted MS/MS data were collected with HCD fragmentation with a normalized collisional energy, NCE, of 35. For untargeted data-dependent methods, the instrument was run with the following MS1 parameters: automatic gain control (AGC) = 2e5 charges, Resolution = 35,000, maximum injection time = 40 ms, scan range = $100-1000 \, m/z$. Tandem MS data were acquired in a data-dependent fashion on the five most abundant precursor ions with a 2 m/z precursor isolation window, a minimum AGC target of 6e3, and dynamic exclusion of previously fragmented precursors set to 4 s.

Transient State Methods. Transient state kinetic characterization of hOAT with 028: A sample of hOAT (17 μ M) was mixed with 5 (0–11 mM) at 20 °C using a rapid mixing stopped-flow spectrophotometer (TgK Scientific) equipped with charge-coupled device (CCD) detection, allowing for the collection time-resolved spectra. The reaction was observed at all wavelengths between 300 and 600 nm for 150 s. A reconstructed time zero point was included in the data and was obtained by adding the spectrum of the enzyme, and the spectrum of the inhibitor when measured separately. The data were fit to a single exponential term describing a one-step irreversible model. Single wavelength traces were extracted from the time-resolved spectra data sets at the wavelengths of maximal absorbance in the initial and final spectra (425 and 320 nm, respectively) to provide a visual comparison of the time dependence of the events at each wavelength.

Docking Study. Docking models of ligands bound to hOAT and GABA-AT were developed utilizing the Molecular Operating Environment (MOE) computational suite's Builder utility s3,54 according to previously reported protocol.

Theoretical p K_a **Calculations.** The theoretical p K_a calculations were performed using previous protocols.³²

ASSOCIATED CONTENT

Solution Supporting Information

The Supporting Information is available free of charge at https://pubs.acs.org/doi/10.1021/acschembio.4c00022.

Molecular docking studies for intermediates in the active site of hOAT, pGABA-AT; inhibitory activities of 5 against hOAT and hGABA-AT; inhibitory activities of 4 against hOAT and hGABA-AT; structure of hOAT homodimer inactivated by 5; time-dependent dialysis of partially or completely inactivated hOAT; comparison of native top-down mass spectra for hOAT; comparison of denatured top-down true individual ion mass spectra for hOAT; data collection and refinement statistics; and NMR spectra and ORTEPs of X-ray structure (PDF)

Accession Codes

The PDB code for X-ray crystal structures described in this study has been deposited in the Protein Data Bank under the following accession code (see Table S1 in the SI for details): 8 V9M.

AUTHOR INFORMATION

Corresponding Author

Richard B. Silverman — Department of Chemistry, Chemistry of Life Processes Institute, and Center for Developmental Therapeutics, Northwestern University, Evanston, Illinois 60208, United States; Department of Molecular Biosciences, Northwestern University, Evanston, Illinois 60208, United States; Department of Pharmacology, Northwestern University, Chicago, Illinois 60611, United States; orcid.org/0000-0001-9034-1084; Phone: +1-847-491-5653; Email: r-silverman@northwestern.edu; Fax: +1 847 491 7713

Authors

Allison N. Devitt — Department of Chemistry, Chemistry of Life Processes Institute, and Center for Developmental Therapeutics, Northwestern University, Evanston, Illinois 60208, United States; orcid.org/0000-0003-2816-7120

Abigail L. Vargas – Department of Chemistry and Biochemistry, Loyola University Chicago, Chicago, Illinois 60660, United States

Wei Zhu – Department of Chemistry, Chemistry of Life Processes Institute, and Center for Developmental Therapeutics, Northwestern University, Evanston, Illinois 60208, United States

Benjamin James Des Soye — Department of Molecular Biosciences, Northwestern University, Evanston, Illinois 60208, United States; orcid.org/0000-0001-5480-4192

Fatma Ayaloglu Butun – Department of Molecular Biosciences, Northwestern University, Evanston, Illinois 60208, United States

Tyler Alt – Department of Chemistry and Biochemistry, Loyola University Chicago, Chicago, Illinois 60660, United States

Nicholas Kaley – Department of Chemistry and Biochemistry, Loyola University Chicago, Chicago, Illinois 60660, United States

Glaucio M. Ferreira — Department of Clinical and Toxicological Analyses, School of Pharmaceutical Sciences, University of São Paulo, São Paulo 05508-000 SP, Brazil; orcid.org/0000-0002-1952-9428 Graham R. Moran – Department of Chemistry and Biochemistry, Loyola University Chicago, Chicago, Illinois 60660, United States; orcid.org/0000-0002-6807-1302

Neil L. Kelleher — Department of Molecular Biosciences, Northwestern University, Evanston, Illinois 60208, United States; © orcid.org/0000-0002-8815-3372

Dali Liu — Department of Chemistry and Biochemistry, Loyola University Chicago, Chicago, Illinois 60660, United States; orcid.org/0000-0002-7587-703X

Complete contact information is available at: https://pubs.acs.org/10.1021/acschembio.4c00022

Author Contributions

[#]A.N.D. and A.L.V. contributed equally to this work.

Notes

The authors declare no competing financial interest.

ACKNOWLEDGMENTS

The authors are grateful to the National Institutes of Health (grants R01 DA030604 and R01 CA260250 to R.B.S. and grants P41 GM108569 and P30 DA018310 to N.L.K.) and the National Science Foundation (grant 1904480 to G.R.M.) for financial support. This work made use of the IMSERC at Northwestern University, which has received support from the Soft and Hybrid Nanotechnology Experimental (SHyNE) Resource (NSF NNCI-1542205), the State of Illinois, and the International Institute for Nanotechnology (IIN). X-ray diffraction data collection used resources of the Advanced Photon Source, a U.S. Department of Energy (DOE) Office of Science User Facility operated for the DOE Office of Science by Argonne National Laboratory under contract no. DE-AC02-06CH11357. The use of LS-CAT Sector 21 was supported by the Michigan Economic Development Corporation and the Michigan Technology Tri-Corridor (grant 085P1000817). G.M.F. is a recipient of a fellowship from FAPESP (Grant # 2021/11205-9), Brazil.

ABBREVIATIONS

hOAT, human ornithine aminotransferase; PLP, pyridoxal S'-phosphate; HCC, hepatocellular carcinoma; α -KG, α -ketoglutarate; GSA, glutamate-5-semialdehyde; L-Glu, L-glutamate; PMP, pyridoxamine-S'-phosphate; PSC, 1-pyrroline-5-carboxylate; PYCR, pyrroline-5-carboxylate reductase; PSCS, pyrroline-5-carboxylate synthase; HIF1 α , hypoxia-inducible factor- 1α ; L-Gln, glutamine; GS, glutamine synthetase; GABA-AT, γ -aminobutyric acid aminotransferase; GABA, γ -aminobutyric acid; MBIs, mechanism-based inactivators

REFERENCES

- (1) Sayiner, M.; Golabi, P.; Younossi, Z. M. Disease Burden of Hepatocellular Carcinoma: A Global Perspective. *Dig. Dis. Sci.* **2019**, 64 (4), 910–917.
- (2) Personeni, N.; Rimassa, L. Hepatocellular Carcinoma: A Global Disease in Need of Individualized Treatment Strategies. *J. Oncol. Pharm. Pract.* **2017**, *13* (6), 368–369.
- (3) Sherman, M.; Bruix, J.; Porayko, M.; Tran, T.; AASLD Practice Guidelines Committee. Screening for hepatocellular carcinoma: The rationale for the American Association for the Study of Liver Diseases recommendations. *Hepatology* **2012**, *56* (3), 793–796, DOI: 10.1002/hep.25869.
- (4) Yang, J. D.; Roberts, L. R. Hepatocellular carcinoma: A global view. *Nat. Rev. Gastroenterol. Hepatol.* **2010**, 7 (8), 448–458.

- (5) She, W. H.; Chok, K. S. Strategies to increase the resectability of hepatocellular carcinoma. *World J. Hepatol.* **2015**, *7* (18), 2147–2154.
- (6) Santopaolo, F.; Lenci, I.; Milana, M.; Manzia, T. M.; Baiocchi, L. Liver transplantation for hepatocellular carcinoma: Where do we stand? *World J. Gastroenterol.* **2019**, 25 (21), 2591–2602.
- (7) Rahimi, R. S.; Trotter, J. F. Liver transplantation for hepatocellular carcinoma: outcomes and treatment options for recurrence. *Ann. Gastroenterol.* **2015**, 28 (3), 323–330.
- (8) Bray, F.; Ferlay, J.; Soerjomataram, I.; Siegel, R. L.; Torre, L. A.; Jemal, A. Global cancer statistics 2018: GLOBOCAN estimates of incidence and mortality worldwide for 36 cancers in 185 countries. *Ca-Cancer J. Clin.* **2018**, *68* (6), 394–424.
- (9) Liu, W.; Le, A.; Hancock, C.; Lane, A. N.; Dang, C. V.; Fan, T. W.; Phang, J. M. Reprogramming of proline and glutamine metabolism contributes to the proliferative and metabolic responses regulated by oncogenic transcription factor c-MYC. *Proc. Natl. Acad. Sci. U.S.A.* 2012, 109 (23), 8983–8988.
- (10) Ginguay, A.; Cynober, L.; Curis, E.; Nicolis, I. Ornithine Aminotransferase, an Important Glutamate-Metabolizing Enzyme at the Crossroads of Multiple Metabolic Pathways. *Biology* **2017**, *6* (1), No. 18, DOI: 10.3390/biology6010018.
- (11) Herzfeld, A.; Knox, W. E. The properties, developmental formation, and estrogen induction of ornithine aminotransferase in rat tissues. *J. Biol. Chem.* **1968**, 243 (12), 3327–3332.
- (12) Peraino, C.; Bunville, L. G.; Tahmisian, T. N. Chemical, physical, and morphological properties of ornithine Aminotransferase from rat liver. *J. Biol. Chem.* **1969**, 244 (9), 2241–2249.
- (13) Shen, Y. A.; Chen, C. C.; Chen, B. J.; Wu, Y. T.; Juan, J. R.; Chen, L. Y.; Teng, Y. C.; Wei, Y. H. Potential Therapies Targeting Metabolic Pathways in Cancer Stem Cells. *Cells* **2021**, *10* (7), No. 1772, DOI: 10.3390/cells10071772.
- (14) Burke, L.; Guterman, I.; Palacios Gallego, R.; Britton, R. G.; Burschowsky, D.; Tufarelli, C.; Rufini, A. The Janus-like role of proline metabolism in cancer. *Cell Death Discovery* **2020**, *6*, 104.
- (15) Tang, L.; Zeng, J.; Geng, P.; Fang, C.; Wang, Y.; Sun, M.; Wang, C.; Wang, J.; Yin, P.; Hu, C.; et al. Global Metabolic Profiling Identifies a Pivotal Role of Proline and Hydroxyproline Metabolism in Supporting Hypoxic Response in Hepatocellular Carcinoma. *Clin. Cancer Res.* **2018**, 24 (2), 474–485.
- (16) Shanware, N. P.; Mullen, A. R.; DeBerardinis, R. J.; Abraham, R. T. Glutamine: pleiotropic roles in tumor growth and stress resistance. *J. Mol. Med.* **2011**, *89* (3), 229–236.
- (17) DeBerardinis, R. J.; Mancuso, A.; Daikhin, E.; Nissim, I.; Yudkoff, M.; Wehrli, S.; Thompson, C. B. Beyond aerobic glycolysis: transformed cells can engage in glutamine metabolism that exceeds the requirement for protein and nucleotide synthesis. *Proc. Natl. Acad. Sci. U.S.A.* **2007**, *104* (49), 19345–19350.
- (18) Cadoret, A.; Ovejero, C.; Terris, B.; Souil, E.; Levy, L.; Lamers, W. H.; Kitajewski, J.; Kahn, A.; Perret, C. New targets of beta-catenin signaling in the liver are involved in the glutamine metabolism. *Oncogene* **2002**, *21* (54), 8293–8301.
- (19) Colnot, S.; Decaens, T.; Niwa-Kawakita, M.; Godard, C.; Hamard, G.; Kahn, A.; Giovannini, M.; Perret, C. Liver-targeted disruption of Apc in mice activates beta-catenin signaling and leads to hepatocellular carcinomas. *Proc. Natl. Acad. Sci. U.S.A.* **2004**, *101* (49), 17216–17221.
- (20) John, R.; Fowler, L. Mammalian o-amino acid transaminases. In *Thnasaminases*; Crhisten, P.; Metzler, D. E., Eds.; 1985.
- (21) Mehta, P. K.; Hale, T. I.; Christen, P. Aminotransferases: demonstration of homology and division into evolutionary subgroups. *Eur. J. Biochem.* **1993**, 214 (2), 549–561.
- (22) Markova, M.; Peneff, C.; Hewlins, M. J.; Schirmer, T.; John, R. A. Determinants of substrate specificity in omega-aminotransferases. *J. Biol. Chem.* **2005**, *280* (43), 36409–36416.
- (23) Storici, P.; Capitani, G.; Muller, R.; Schirmer, T.; Jansonius, J. N. Crystal structure of human ornithine aminotransferase complexed with the highly specific and potent inhibitor 5-fluoromethylornithine. *J. Mol. Biol.* **1999**, 285 (1), 297–309.

- (24) Silverman, R. B. Design and Mechanism of GABA Aminotransferase Inactivators. Treatments for Epilepsies and Addictions. *Chem. Rev.* **2018**, *118* (7), 4037–4070.
- (25) Silverman, R. B. Mechanism-based enzyme inactivators. *Methods Enzymol* **1995**, 249, 240–283.
- (26) Pan, Y.; Gerasimov, M. R.; Kvist, T.; Wellendorph, P.; Madsen, K. K.; Pera, E.; Lee, H.; Schousboe, A.; Chebib, M.; Brauner-Osborne, H.; et al. (1S, 3S)-3-amino-4-difluoromethylenyl-1-cyclopentanoic acid (CPP-115), a potent gamma-aminobutyric acid aminotransferase inactivator for the treatment of cocaine addiction. *J. Med. Chem.* **2012**, *5S* (1), 357–366.
- (27) Lee, H.; Le, H. V.; Wu, R.; Doud, E.; Sanishvili, R.; Kellie, J. F.; Compton, P. D.; Pachaiyappan, B.; Liu, D.; Kelleher, N. L.; Silverman, R. B. Mechanism of Inactivation of GABA Aminotransferase by (E)-and (Z)-(1S,3S)-3-Amino-4-fluoromethylenyl-1-cyclopentanoic Acid. ACS Chem. Biol. 2015, 10 (9), 2087–2098. From NLM Medline.
- (28) Juncosa, J. I.; Takaya, K.; Le, H. V.; Moschitto, M. J.; Weerawarna, P. M.; Mascarenhas, R.; Liu, D.; Dewey, S. L.; Silverman, R. B. Design and Mechanism of (S)-3-Amino-4-(difluoromethylenyl)cyclopent-1-ene-1-carboxylic Acid, a Highly Potent gamma-Aminobutyric Acid Aminotransferase Inactivator for the Treatment of Addiction. *J. Am. Chem. Soc.* 2018, 140 (6), 2151–2164
- (29) Zigmond, E.; Ben Ya'acov, A.; Lee, H.; Lichtenstein, Y.; Shalev, Z.; Smith, Y.; Zolotarov, L.; Ziv, E.; Kalman, R.; Le, H. V.; et al. Suppression of Hepatocellular Carcinoma by Inhibition of Overexpressed Ornithine Aminotransferase. *ACS Med. Chem. Lett.* **2015**, 6 (8), 840–844.
- (30) Zhu, W.; Doubleday, P. F.; Catlin, D. S.; Weerawarna, P. M.; Butrin, A.; Shen, S.; Wawrzak, Z.; Kelleher, N. L.; Liu, D.; Silverman, R. B. A Remarkable Difference That One Fluorine Atom Confers on the Mechanisms of Inactivation of Human Ornithine Aminotransferase by Two Cyclohexene Analogues of gamma-Aminobutyric Acid. J. Am. Chem. Soc. 2020, 142 (10), 4892–4903.
- (31) Zhu, W.; Doubleday, P. F.; Butrin, A.; Weerawarna, P. M.; Melani, R. D.; Catlin, D. S.; Dwight, T. A.; Liu, D.; Kelleher, N. L.; Silverman, R. B. Remarkable and Unexpected Mechanism for (S)-3-Amino-4-(difluoromethylenyl)cyclohex-1-ene-1-carboxylic Acid as a Selective Inactivator of Human Ornithine Aminotransferase. *J. Am. Chem. Soc.* **2021**, *143* (21), 8193–8207.
- (32) Zhu, W.; Butrin, A.; Melani, R. D.; Doubleday, P. F.; Ferreira, G. M.; Tavares, M. T.; Habeeb Mohammad, T. S.; Beaupre, B. A.; Kelleher, N. L.; Moran, G. R.; et al. Rational Design, Synthesis, and Mechanism of (3S,4R)-3-Amino-4-(difluoromethyl)cyclopent-1-ene-1-carboxylic Acid: Employing a Second-Deprotonation Strategy for Selectivity of Human Ornithine Aminotransferase over GABA Aminotransferase. J. Am. Chem. Soc. 2022, 144 (12), 5629–5642.
- (33) Shen, S.; Butrin, A.; Doubleday, P. F.; Melani, R. D.; Beaupre, B. A.; Tavares, M. T.; Ferreira, G. M.; Kelleher, N. L.; Moran, G. R.; Liu, D.; Silverman, R. B. Turnover and Inactivation Mechanisms for (S)-3-Amino-4,4-difluorocyclopent-1-enecarboxylic Acid, a Selective Mechanism-Based Inactivator of Human Ornithine Aminotransferase. *J. Am. Chem. Soc.* **2021**, *143* (23), 8689–8703.
- (34) Zhu, W.; Butrin, A.; Melani, R. D.; Doubleday, P. F.; Ferreira, G. M.; Tavares, M. T.; Habeeb Mohammad, T. S.; Beaupre, B. A.; Kelleher, N. L.; Moran, G. R.; et al. Rational Design, Synthesis, and Mechanism of (3S,4R)-3-Amino-4-(difluoromethyl)cyclopent-1-ene1-carboxylic Acid: Employing a Second-Deprotonation Strategy for Selectivity of Human Ornithine Aminotransferase over GABA Aminotransferase. *J. Am. Chem. Soc.* 2022, 144 (12), 5629–5642.
- (35) Trongsiriwat, N.; Li, M. Y.; Pascual-Escudero, A.; Yucel, B.; Walsh, P. J. Palladium-Catalyzed Allylic Alkylation of 2-Aryl-1,3-Dithianes, an Umpolung Synthesis of β , γ -Unsaturated Ketones. *Adv. Synth. Catal* **2019**, 361 (3), 502–509.
- (36) Barral, K.; Courcambeck, J.; Pepe, G.; Balzarini, J.; Neyts, J.; De Clercq, E.; Camplo, M. Synthesis and antiviral evaluation of cissubstituted cyclohexenyl and cyclohexanyl nucleosides. *J. Med. Chem.* **2005**, 48 (2), 450–456.

- (37) Yeung, Y. Y.; Gao, X.; Corey, E. J. A general process for the haloamidation of olefins. Scope and mechanism. *J. Am. Chem. Soc.* **2006**, *128* (30), 9644–9645.
- (38) Butrin, A.; Butrin, A.; Wawrzak, Z.; Moran, G. R.; Liu, D. Determination of the pH dependence, substrate specificity, and turnovers of alternative substrates for human ornithine aminotransferase. *J. Biol. Chem.* **2022**, 298 (6), No. 101969.
- (39) Danielson, M. A.; Falke, J. J. Use of 19F NMR to probe protein structure and conformational changes. *Annu. Rev. Biophys. Biomol. Struct.* **1996**, 25, 163–195.
- (40) Martinez, D.; Gerig, J. T. Intermolecular (1)H[(19)F] NOEs in studies of fluoroalcohol-induced conformations of peptides and proteins. *J. Magn. Reson.* **2001**, *152* (2), 269–275.
- (41) Bissantz, C.; Kuhn, B.; Stahl, M. A medicinal chemist's guide to molecular interactions. *J. Med. Chem.* **2010**, *53* (14), 5061–5084.
- (42) Pham, T. V.; Murkin, A. S.; Moynihan, M. M.; Harris, L.; Tyler, P. C.; Shetty, N.; Sacchettini, J. C.; Huang, H. L.; Meek, T. D. Mechanism-based inactivator of isocitrate lyases 1 and 2 from Mycobacterium tuberculosis. *Proc. Natl. Acad. Sci. U.S.A.* **2017**, *114* (29), 7617–7622.
- (43) Frieden, E.; Walter, C. Prevalence and significance of the product inhibition of enzymes. *Nature* **1963**, *198*, 834–837.
- (44) Lee, H.; Doud, E. H.; Wu, R.; Sanishvili, R.; Juncosa, J. I.; Liu, D.; Kelleher, N. L.; Silverman, R. B. Mechanism of inactivation of gamma-aminobutyric acid aminotransferase by (1S,3S)-3-amino-4-difluoromethylene-1-cyclopentanoic acid (CPP-115). *J. Am. Chem. Soc.* 2015, 137 (7), 2628–2640.
- (45) Wheless, J. W.; Ramsay, R. E.; Collins, S. D. Vigabatrin. *Neurotherapeutics* **2007**, 4 (1), 163–172.
- (46) Mascarenhas, R.; Le, H. V.; Clevenger, K. D.; Lehrer, H. J.; Ringe, D.; Kelleher, N. L.; Silverman, R. B.; Liu, D. Selective Targeting by a Mechanism-Based Inactivator against Pyridoxal 5'-Phosphate-Dependent Enzymes: Mechanisms of Inactivation and Alternative Turnover. *Biochemistry* **2017**, *56* (37), 4951–4961.
- (47) Moschitto, M. J.; Doubleday, P. F.; Catlin, D. S.; Kelleher, N. L.; Liu, D.; Silverman, R. B. Mechanism of Inactivation of Ornithine Aminotransferase by (1S,3S)-3-Amino-4-(hexafluoropropan-2-ylidenyl)cyclopentane-1-carboxylic Acid. *J. Am. Chem. Soc.* **2019**, 141 (27), 10711–10721.
- (48) Vonrhein, C.; Flensburg, C.; Keller, P.; Sharff, A.; Smart, O.; Paciorek, W.; Womack, T.; Bricogne, G. Data processing and analysis with the autoPROC toolbox. *Acta Crystallogr., Sect. D: Biol. Crystallogr.* **2011**, *67* (Pt 4), 293–302.
- (49) McCoy, A. J.; Grosse-Kunstleve, R. W.; Adams, P. D.; Winn, M. D.; Storoni, L. C.; Read, R. J. Phaser crystallographic software. *J. Appl. Crystallogr.* **2007**, *40* (Pt 4), 658–674.
- (50) Liebschner, D.; Afonine, P. V.; Baker, M. L.; Bunkoczi, G.; Chen, V. B.; Croll, T. I.; Hintze, B.; Hung, L. W.; Jain, S.; McCoy, A. J.; et al. Macromolecular structure determination using X-rays, neutrons and electrons: recent developments in Phenix. *Acta Crystallogr., Sect. D: Struct. Biol.* **2019**, 75 (Pt 10), 861–877.
- (51) Emsley, P.; Lohkamp, B.; Scott, W. G.; Cowtan, K. Features and development of Coot. *Acta Crystallogr., Sect. D: Biol. Crystallogr.* **2010**, *66* (Pt 4), 486–501.
- (52) Pettersen, E. F.; Goddard, T. D.; Huang, C. C.; Couch, G. S.; Greenblatt, D. M.; Meng, E. C.; Ferrin, T. E. UCSF Chimera-a visualization system for exploratory research and analysis. *J. Comput. Chem.* **2004**, 25 (13), 1605–1612.
- (53) Heath, T. K.; Lutz, M. R., Jr.; Reidl, C. T.; Guzman, E. R.; Herbert, C. A.; Nocek, B. P.; Holz, R. C.; Olsen, K. W.; Ballicora, M. A.; Becker, D. P. Practical spectrophotometric assay for the dapEencoded N-succinyl-L,L-diaminopimelic acid desuccinylase, a potential antibiotic target. *PLoS One* **2018**, *13* (4), No. e0196010.
- (54) Vilar, S.; Cozza, G.; Moro, S. Medicinal chemistry and the molecular operating environment (MOE): application of QSAR and molecular docking to drug discovery. *Curr. Top Med. Chem.* **2008**, 8 (18), 1555–1572.